BeBeC-2026-S12

RECENT AIRCRAFT FLYOVER MEASUREMENTS IN CHINA: DESIGN, IMPLEMENTATION, AND DATA PROCESSING

Haoyuan Dong[1], Cheng Wei Lee[1], Yuqi Zhou[1] and Wei Ma[1]
[1]School of Aeronautics and Astronautics, Shanghai Jiao Tong University
800 Dongchuan Road, Shanghai 200240, P.R. China
Contact: mawei@sjtu.edu.cn

Abstract

Aircraft flyover measurements have become a standard practice in the research and development of mainstream large civil aircraft. As China's large civil aircraft programs have advanced, these measurement techniques have garnered growing domestic attention. This paper presents a full-scale aircraft flyover measurement workflow for large civil aircraft, encompassing microphone array design and calibration, noise acquisition, aircraft trajectory determination, and data processing. For the measurements, a large-scale nested microphone array is deployed to synchronously capture multichannel acoustic pressure signals during aircraft flyovers. To enhance the efficiency of large-scale field tests, computer vision-based methods are additionally integrated to enable rapid microphone position calibration and aircraft trajectory reconstruction. Finally, the measured flyover noise data are processed using MCB-GT to generate high-resolution acoustic source maps, and source-region integration is demonstrated for a representative one-third-octave band to illustrate the relative contributions of major noise-source regions.

1 INTRODUCTION

As global air transport continues to grow, aircraft noise has become an increasingly important issue affecting airport communities and the sustainable development of civil aviation. In March 2026, the International Civil Aviation Organization (ICAO) Council adopted a revised aircraft noise standard that reduces the permissible noise levels for large aircraft categories by 6 decibels (dB) [1], which will apply to new aircraft type designs as of 2029. This development highlights aircraft noise reduction as a critical requirement for the green development of next-generation civil aircraft. Achieving effective noise reduction requires accurate characterization of the spatial distribution and relative strengths of airframe and propulsion noise sources. Aircraft flyover measurements use large ground-based microphone arrays to record acoustic pressure signals

during aircraft flyovers, enabling source localization on full-scale aircraft under realistic flight conditions and supporting both noise-mechanism studies and low-noise design [2].

The development of aircraft flyover measurement techniques has been closely associated with field tests on representative full-scale aircraft platforms. In the 1990s, Michel and colleagues at the German Aerospace Center (DLR) pioneered the use of large-aperture microphone arrays for outdoor aircraft flyover measurements [3, 4, 5]. Their work demonstrated the feasibility of localizing dominant aircraft noise sources under realistic flight conditions and laid the foundation for subsequent studies. From 2001 to 2005, NASA and Boeing conducted a series of Boeing 777 flight tests to acquire full-scale acoustic datasets and evaluate aircraft noise-reduction concepts [6]. In 2002, DLR and ONERA performed A340 flyover source-localization measurements using a 16 m $\times$ 16 m phased microphone array composed of 161 microphones. The study showed that nested arrays are required for reliable localization over a wide frequency range [2]. From 2004 to 2008, DLR carried out several flyover campaigns at Parchim Airport, including measurements on representative aircraft such as the Airbus A319 and Boeing 747-400, providing databases for noise source identification and noise prediction model validation [7]. In 2012, Bombardier and the Université de Sherbrooke acoustics group conducted a flyover campaign at Montréal–Trudeau International Airport, where a microphone array and two synchronized cameras were used to acquire acoustic and trajectory data from multiple CRJ overflights [8]. More recently, DLR conducted flyover measurements on the Airbus A320-232 ATRA research aircraft, using large multi-arm spiral arrays together with laser ranging and onboard GNSS data to improve trajectory reconstruction and source localization accuracy [9, 10]. Related campaigns on modified ATRA configurations further supported the acoustic assessment of noise-reduction technologies. In parallel, NASA and Boeing performed full-scale flyover tests on aircraft such as the Boeing 737 MAX-7 and 787-10, extending flyover measurements to the evaluation of advanced inlet liners, fan-noise characteristics, and aircraft system noise under flight conditions [11, 12].

In China, aircraft flyover measurements were first applied during the development of the C909 regional jet, formerly known as the ARJ21. Between 2012 and 2013, Chen et al. performed flyover measurements and array data analysis for different flight phases of the C909, quantifying the noise contributions of key components such as the landing gear and high-lift devices under various operating conditions [13, 14, 15]. This work provided the earliest domestic experience in civil aircraft flyover noise measurements. However, compared with regional aircraft, large civil aircraft impose more stringent requirements on array deployment, synchronous multichannel acquisition, geometric calibration, trajectory reconstruction, and moving-source localization. A systematic measurement and processing framework is therefore required to support full-scale flyover noise testing for large civil aircraft.

To address these challenges, this paper presents a comprehensive aircraft flyover measurement framework for large civil aircraft. The proposed framework consists of four main stages: microphone array design and calibration, noise acquisition, aircraft trajectory determination, and data processing. It integrates large-scale microphone array measurements, computer vision-based geometric calibration and trajectory reconstruction, and moving-source acoustic imaging to support high-resolution source localization and quantitative analysis of major aircraft noise source regions.

The remainder of this paper is organized as follows. Section 2 introduces the overall workflow of the proposed measurement framework. Section 3 describes the microphone array design

and calibration method. Section 4 presents the noise acquisition system. Section 5 explains the aircraft trajectory determination method. Section 6 describes the data processing procedure for source localization and quantitative source-region analysis. Finally, Section 7 summarizes the main conclusions.

2 OVERALL WORKFLOW

This section outlines the complete workflow for full-scale aircraft flyover measurements. As shown in Fig. 1, the workflow consists of four main stages: microphone array design and calibration, noise acquisition, aircraft trajectory determination, and data processing.

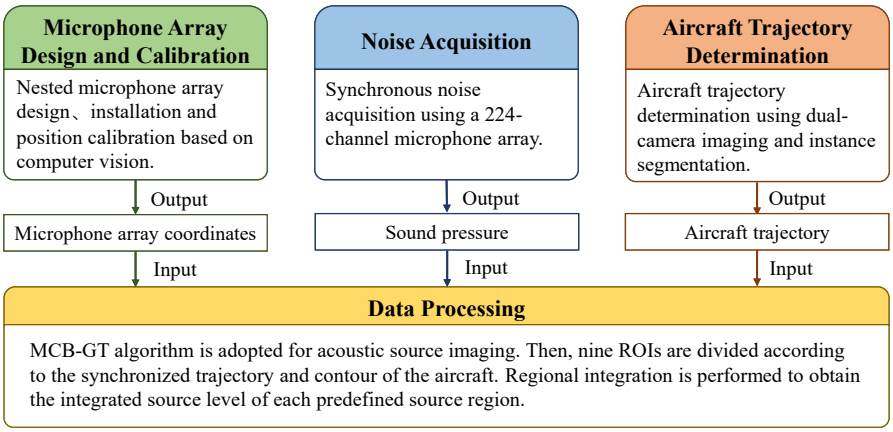

Figure 1: Aircraft flyover measurement workflow.

In the first stage, a nested microphone array is designed and deployed in the field, and its microphone positions are calibrated using a computer vision-based method to obtain accurate array element coordinates. In the second stage, the 224-channel microphone array is used to synchronously acquire multichannel acoustic pressure signals during aircraft flyovers. In parallel, a stereo imaging system combined with instance segmentation is used to track the aircraft and reconstruct its three-dimensional trajectory. Finally, the calibrated array coordinates, acoustic pressure signals, and reconstructed aircraft trajectory are used as unified inputs for MCB-GT-based acoustic imaging. The resulting source maps are further refined by deconvolution and then analyzed through region-of-interest (ROI) integration to quantify and rank the contributions of the major aircraft noise source regions.

3 MICROPHONE ARRAY DESIGN AND CALIBRATION

3.1 Array Design and Field Deployment

The microphone array used for aircraft flyover measurements must provide sufficient low-frequency resolution while maintaining accurate source localization over the mid- and high-frequency ranges. The low-frequency performance is mainly determined by the array aperture, whereas mid- and high-frequency beamforming requires a higher spatial sampling density and

an appropriate planar sensor distribution. Owing to limitations in the number of acquisition channels and practical constraints in field deployment, a single array configuration generally involves trade-offs between low-frequency aperture, high-frequency spatial sampling, and practical deployability. Therefore, an optimized nested array consisting of an inner subarray and an outer subarray is adopted in this study [16].

As shown in Fig. 2(a), the inner subarray adopts a seven-arm spiral configuration with an effective aperture of 2 m and contains 112 microphones. This subarray provides the spatial sampling density required for source localization in the mid- and high-frequency ranges. The outer subarray consists of another 112 microphones arranged in a modular straight-arm configuration, extending the overall aperture of the array to 14.5 m and thereby improving the low-frequency source resolution. This nested configuration combines the broadband localization capability of the inner spiral subarray with the large-aperture coverage and practical deployability of the outer straight-arm subarray, making it suitable for repeated outdoor flyover measurements.

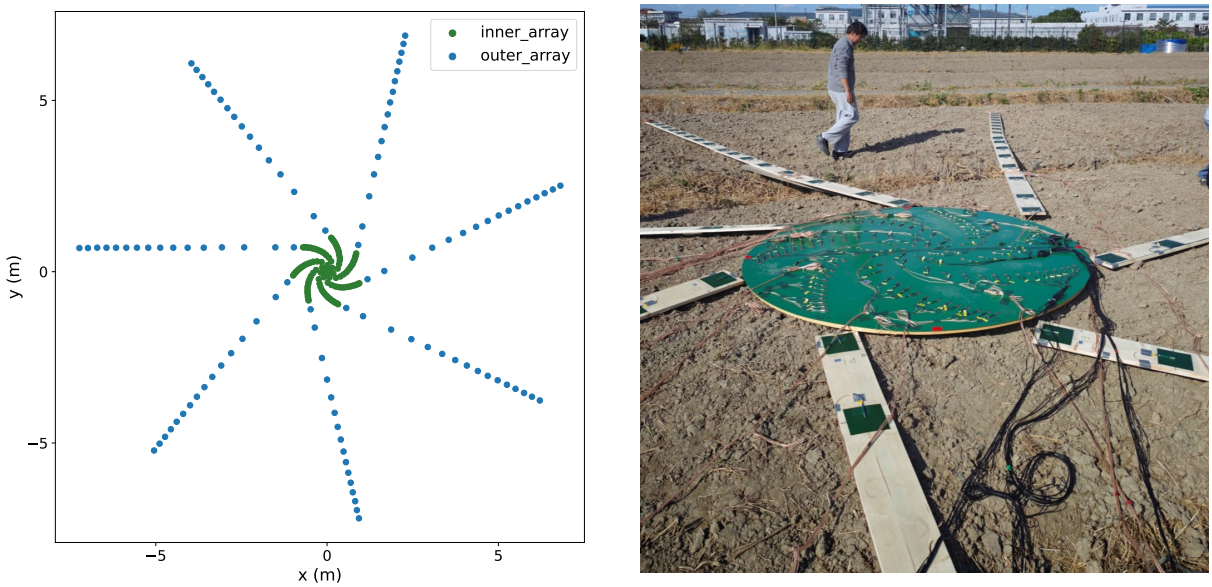

Figure 2: Nested microphone array: (a) array design and (b) field installation.

Figure 2(b) shows the field deployment of the array. To improve deployment efficiency and reduce installation errors, the inner subarray is pre-assembled and transported as an integrated unit, whereas the outer subarray is assembled on site using modular straight-arm units. After deployment, the channel mapping, connectivity, and numbering of all microphones are checked before aircraft flyovers to ensure consistency between the array geometry and the multichannel acquisition system.

3.2 Microphone Position Calibration

In aircraft flyover measurements, the geometric accuracy of the microphone array directly affects the reliability of subsequent beamforming. Deviations between the actual and designed microphone positions can degrade phase matching among array channels, leading to reduced focusing quality in the acoustic source maps and decreased localization accuracy. To address

this issue, a computer vision-based microphone position calibration method is employed in this study.

High-resolution images covering the outer subarray are first acquired in the field. The raw images are corrected for lens distortion and transformed into a planar representation of the array with a uniform scale. The regions corresponding to the reflector plates are then extracted according to their color and contour features, and the center positions of these regions are identified as the microphone positions in the image plane. Finally, the physical coordinates of the outer-array microphones are obtained through the mapping between the image coordinate system and the array coordinate system.

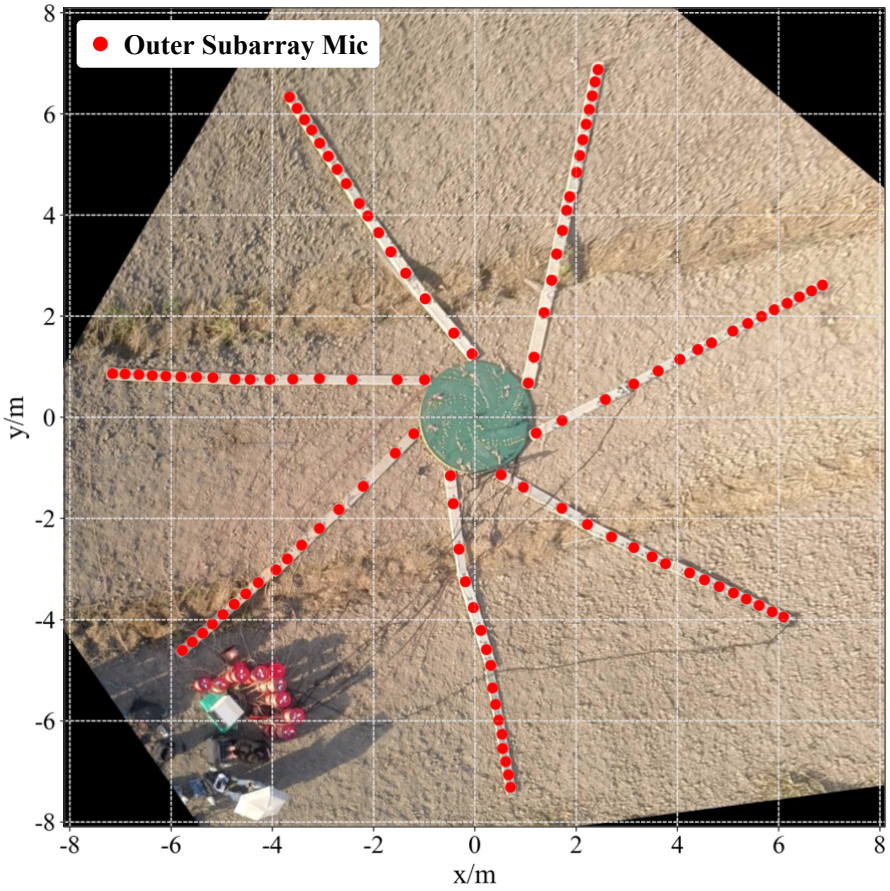

Figure 3: Microphone position calibration for the outer subarray.

Since the inner subarray is prefabricated as an integrated unit, its internal relative geometry remains nearly unchanged after deployment. Therefore, geometric calibration is performed only for the outer subarray, as shown in Fig. 3. To validate the calibration results, the positions of the 112 outer-array microphones are measured individually using high-precision surveying equipment. The comparison shows a mean coordinate deviation of 0.076 m between the point-by-point surveying results and the vision-derived coordinates, corresponding to approximately 0.52% of the full array aperture. Previous work has shown that this level of installation error satisfies the basic geometric accuracy requirements for source localization with large-scale

microphone arrays [17]. Compared with manual point-by-point surveying, the proposed vision-based method substantially reduces field calibration time and operational complexity, making it suitable for rapid calibration of large outdoor arrays.

4 NOISE ACQUISITION

The flyover noise acquisition system consists of microphones, data acquisition hardware, and a host computer. The array is equipped with 224 PCB 130F22 microphones for multichannel acoustic pressure measurements. These microphones provide a broad effective frequency response and therefore meet the frequency-range requirements of aircraft flyover noise tests. The data acquisition system is built on the National Instruments (NI) PXIe platform, including one PXIe-8880 controller, fourteen PXIe-4497 data acquisition cards, and one PXIe-1085 18-slot chassis. This configuration enables synchronous acquisition, centralized control, and high-speed data transmission for all 224 channels.

During each field test, all 224 channels were recorded continuously at a sampling frequency of 51.2 kHz with 24-bit resolution. GPS pulse-per-second signals were recorded by the acquisition system as a common synchronization reference, while absolute timestamps were logged simultaneously by the host computer. This configuration ensured temporal alignment among all acoustic channels and provided a reliable basis for synchronizing the acoustic data with the reconstructed aircraft trajectory during data processing. The noise acquisition field setup is shown in Fig. 4.

5 AIRCRAFT TRAJECTORY DETERMINATION

5.1 Image Acquisition System

The image acquisition system for aircraft trajectory determination is based on two synchronized large-baseline stereo cameras used to capture aircraft flyovers. The system consists of two industrial cameras, a network switch, and a host computer. Both cameras are connected to the shared network switch via Ethernet cables, and the switch is connected to the host computer for simultaneous image acquisition and storage. Basler acA1300-60gc industrial cameras equipped with C23-0824-5M-P lenses are used in this study. Each frame is assigned a hardware-generated timestamp, while the host computer records a GPS-based absolute time. These two time references are combined to establish a unified time base, ensuring accurate synchronization between the reconstructed trajectory and the acoustic measurements during data processing.

Trajectory reconstruction is performed in the same coordinate system as the microphone array to ensure spatial consistency with the array-based source localization results. The origin is defined at the center of the inner subarray, with the array plane located at $z = 0$, and the coordinate axes are aligned with the orientation of the microphone array. As shown in Fig. 5, the two cameras are placed on the ground with a fixed baseline, and their optical axes are oriented to provide a stable overlapping field of view above the array. Previous studies have demonstrated the feasibility of large-baseline stereo systems for aircraft flyover trajectory measurement [8]. Based on this configuration, a trajectory determination pipeline is adopted. It consists of camera calibration, image-plane localization, and stereo reconstruction of the three-dimensional aircraft trajectory.

Figure 4: Field setup of the aircraft flyover noise acquisition.

5.2 Camera Calibration

Both cameras are calibrated using Zhang's standard planar checkerboard method [18]. Multiple checkerboard images captured at different orientations and distances are used to estimate the intrinsic parameters, extrinsic parameters, and lens distortion coefficients of the cameras. The calibrated parameters are then used to correct lens distortion in the raw images, providing geometrically corrected image data for subsequent aircraft image-plane localization.

5.3 Image-Plane Localization

Traditional object detection methods can be sensitive to changes in viewing angle, aircraft attitude, and aircraft configuration. Under such conditions, the center of a bounding box may

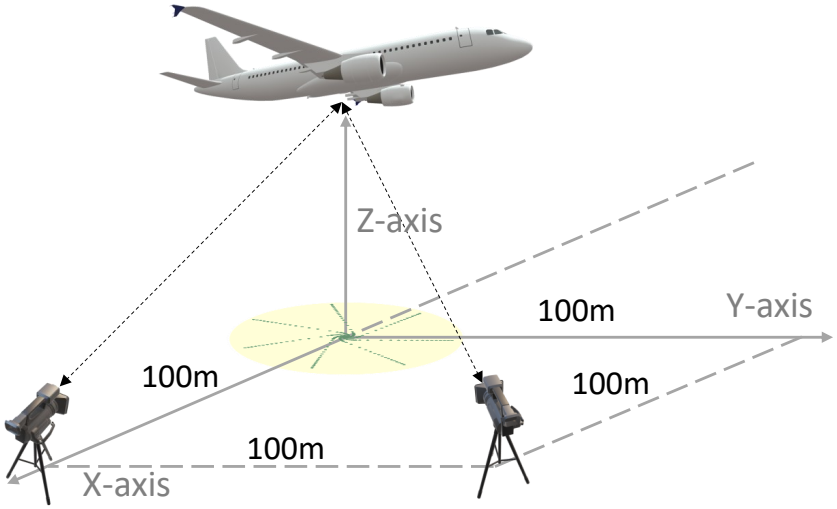

Figure 5: Image acquisition system and coordinate definition.

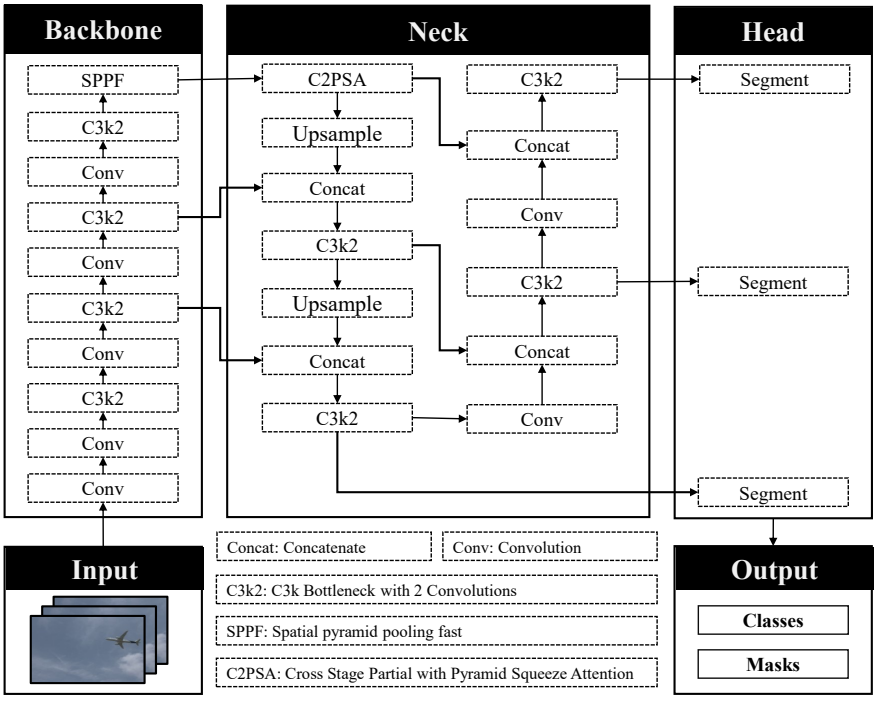

Figure 6: YOLO11 model architecture.

deviate from a representative image-plane position of the aircraft. Therefore, this study employs an instance segmentation approach based on a You Only Look Once (YOLO) model [19]. As shown in Fig. 6, the network consists of a backbone, a neck, and a head, which perform feature extraction, multi-scale feature fusion, and mask/detection prediction, respectively.

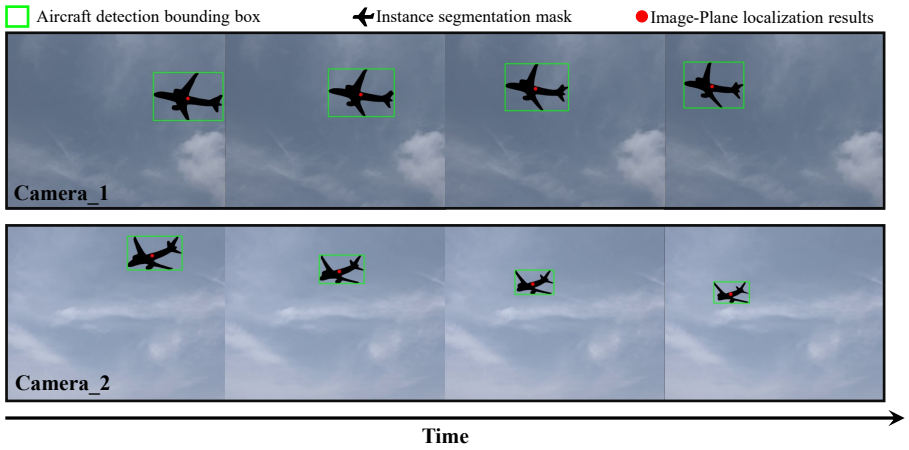

Figure 7: Image-plane localization procedure using instance segmentation.

Representative time-sequential image-plane localization results from the two cameras are shown in Fig. 7. For each frame, the aircraft is first detected with a bounding box, and its silhouette is then extracted as a segmentation mask using YOLO11. The geometric centroid of the mask, marked by the red dot, is taken as the aircraft image-plane position. Compared with the bounding-box center, the mask centroid provides a more robust estimate of the aircraft image-plane position under variations in viewing angle, attitude, and configuration.

5.4 Trajectory Reconstruction

Using the synchronized image-plane positions from the two cameras, the three-dimensional aircraft position is reconstructed through stereo triangulation. The two-dimensional image coordinates are back-projected into spatial rays using the calibrated intrinsic and extrinsic camera parameters. Owing to measurement noise, the two rays generally do not intersect exactly. Therefore, the midpoint of the shortest line segment connecting the two rays is used as the optimal three-dimensional position estimate for each frame. Applying this procedure to all synchronized image pairs yields a discrete three-dimensional trajectory, which is subsequently interpolated and smoothed to obtain a continuous and stable flight path for acoustic source localization.

5.5 Error Analysis

To quantitatively evaluate the accuracy of the proposed trajectory determination method, flight height above the array plane and speed are selected as evaluation metrics. The reconstructed results are compared with the corresponding onboard reference data recorded at the same time instants. As shown in Fig. 8, the reconstructed height and speed agree well with the onboard reference data in terms of temporal trends, indicating that the proposed method can effectively capture the aircraft motion during flyover.

The statistical error metrics are summarized in Table 1, including the mean absolute error (MAE), root mean square error (RMSE), and mean absolute percentage error (MAPE). The reconstructed height achieves meter-level accuracy, while the speed error remains within a few

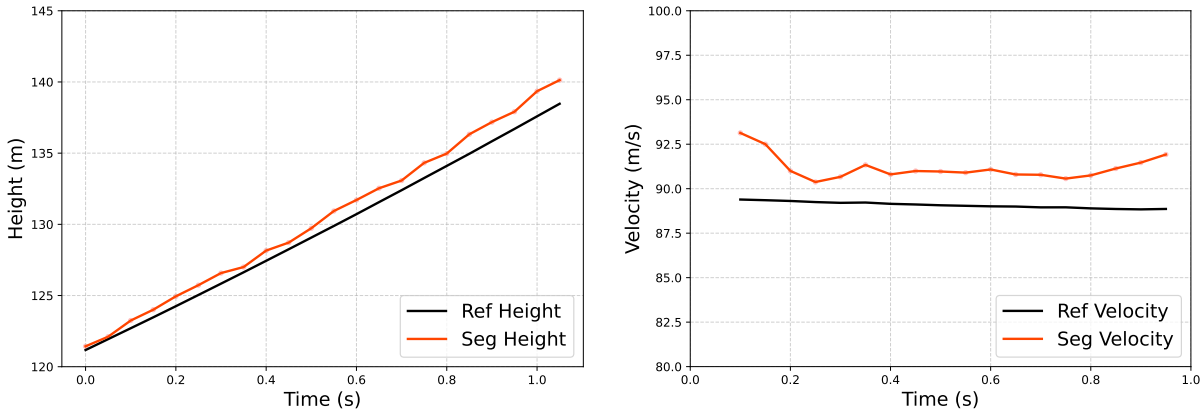

Figure 8: Comparison between the reconstructed trajectory and onboard reference data: (a) height and (b) speed.

Table 1: Accuracy metrics of the reconstructed trajectory.

Flight parameter	MAE	RMSE	MAPE
Height	0.86 m	0.95 m	0.65%
Speed	2.10 m/s	2.19 m/s	2.35%

meters per second. These results indicate that the reconstructed trajectory agrees well with the onboard reference data and provides a consistent trajectory input for the subsequent noise data processing..

6 DATA PROCESSING

This section describes the data analysis procedure used for the localization and quantitative evaluation of aircraft flyover noise sources. The microphone data are first analyzed with the MCB-GT algorithm to obtain beamforming source maps for moving sources. The beamforming results are then post-processed with a DAMAS-compatible deconvolution procedure adapted for MCB-GT moving-source maps in order to improve the spatial resolution and dynamic range of the maps. Finally, the deconvolved maps are integrated over predefined source regions on the aircraft, and the resulting source levels are used to compare and rank the contributions of individual noise-source regions.

6.1 MCB-GT-Based Acoustic Source Localization

For the evaluation of the microphone data, flyover records with incomplete trajectory information or abnormal microphone signals were excluded from the analysis.A uniform ground-plane correction of -6 dB was applied to the microphone spectra before the source-localization analysis to approximate the pressure-doubling effect of ground-mounted microphones. More detailed modelling of frequency-dependent ground reflection and incidence-angle effects was not included in the present analysis. The spectra and source maps obtained from different fly-

overs were subsequently referred to a common distance of 120 m in order to compare cases with different aircraft-to-array distances, following established practice in aircraft flyover array measurements [20]. This normalization accounts for the geometrical spreading of sound under a free-field assumption.

The acoustic source maps were calculated using the MCB-GT algorithm proposed by Zhang [21]. In contrast to conventional beamforming methods based on fixed propagation-delay compensation, MCB-GT is formulated for moving sources and accounts for both the Doppler effect and the time-varying propagation geometry during the flyover.

Assume that the array consists of M microphones, and let the position of the m-th microphone be denoted by $\boldsymbol{x}_m$, where $m = 1,2,\ldots,M$. Let $\boldsymbol{y}_s$ denote the position vector of the s-th scan point, and let ω be the target angular frequency. For each scan point $\boldsymbol{y}_s$ on the aircraft-fixed scanning plane, the instantaneous propagation distance $r_{m,s}(\tau)$ between the source position on the reconstructed trajectory and the m-th microphone is determined from the array geometry and the aircraft trajectory. Based on this time-dependent propagation geometry, shifted-mode transfer functions are constructed, and the MCB-GT beamforming output at the s-th scan point and angular frequency ω is given by

$$B(\boldsymbol{y}_s,\omega) = \frac{1}{M}\left|\sum_{m=1}^{M}\sum_{m_0=-M_0/2}^{M_0/2-1} a_{m_0}^{*}(\boldsymbol{x}_m,\boldsymbol{y}_s,\omega)\,\tilde{p}\left(\boldsymbol{x}_m,\omega+m_0\frac{2\pi}{T}\right)\right|^2, \tag{1}$$

where m_0 is the shifted modal order, M_0 is the total number of retained shifted modes, $a_{m_0}(\boldsymbol{x}_m,\boldsymbol{y}_s,\omega)$ denotes the transfer function of the m_0-th shifted mode, $(\cdot)^*$ denotes complex conjugation, and $\tilde{p}(\boldsymbol{x}_m,\omega+m_0 2\pi/T)$ is the measured pressure spectrum at the shifted angular frequency. Here, T denotes the sampling duration. Further details on the theoretical derivation and the selection of M_0 can be found in [21, 22].

Figure 9 shows a typical projected acoustic source map for the one-third-octave band centered at 2500 Hz. Prominent source regions are observed near the wings, engines, and landing gear. The distribution is consistent with the typical source locations of aircraft approach noise. Owing to the finite spatial resolution of the microphone array, the source regions associated with the main landing gear and the engines are not fully separated in the beamforming map.

The beamforming maps were further processed using a DAMAS-compatible deconvolution procedure adapted for MCB-GT moving-source maps, following the formulation proposed by Zhang and Ma [23]. The deconvolution reduces sidelobes and spatial smearing in the beamforming maps and provides source maps with improved spatial resolution for the subsequent integration over aircraft source regions.

6.2 Source-Region Integration and Contribution Analysis

The deconvolved source maps were divided into a set of predefined integration regions in order to relate the acoustic source distribution to physically meaningful aircraft components. The regions were defined on the aircraft-fixed source map using the synchronized aircraft trajectory, the projected aircraft contour, and the expected locations of the main airframe and propulsion noise sources. As shown in Fig. 10, the integration regions include the left and right slats, left and right flaps, left and right main landing gear, left and right engines, and the nose landing gear. The slat and flap regions are placed along the leading and trailing edges of the wings,

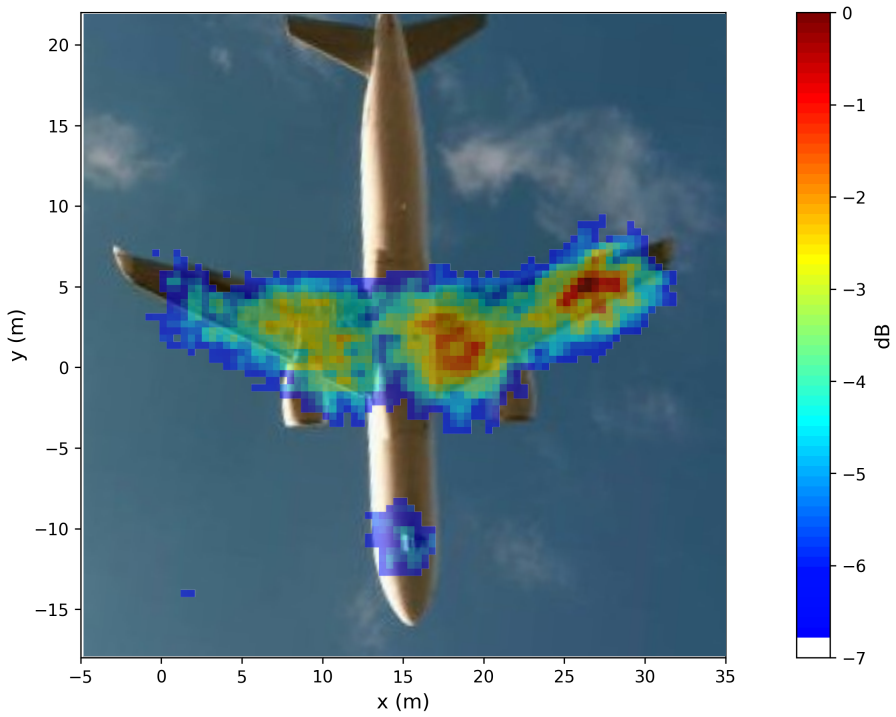

Figure 9: Source map for the one-third-octave band centered at 2500 Hz.

respectively. The main landing gear regions cover the gear bays and wheel assemblies, the engine regions cover the projected locations of the engine nacelles, and the nose landing gear region is defined around the forward lower fuselage.

As a reference level, the far-field SPL was calculated from the energetic mean of the mean-square acoustic pressures measured by the 112 microphones in the inner subarray. It should be noted that this level is not strictly equivalent to the ROI-integrated source levels, because the latter are obtained from deconvolved source maps over predefined aircraft regions and therefore depend on the imaging and integration procedures. Therefore, differences between the far-field SPL and the ROI-integrated total level are expected and are used here only as a qualitative reference.

Figure 11 compares the far-field SPL, the total ROI-integrated level, and the integrated levels of the individual source regions for the one-third-octave band centered at 2500 Hz. The far-field SPL is calculated directly from the energetic mean of the inner-subarray microphone signals. Among the individual ROIs, the highest integrated levels are obtained for the right slats, right main landing gear, and right flaps. Rather than merely indicating a ranking of intrinsic source strengths, this asymmetry suggests that the dominant noise radiation in this frequency band and viewing angle is likely influenced by the aircraft attitude and the relative exposure of the right-side high-lift devices and landing gear to the microphone array. In contrast, the engine regions and the nose landing gear show lower integrated levels, indicating that their contributions are

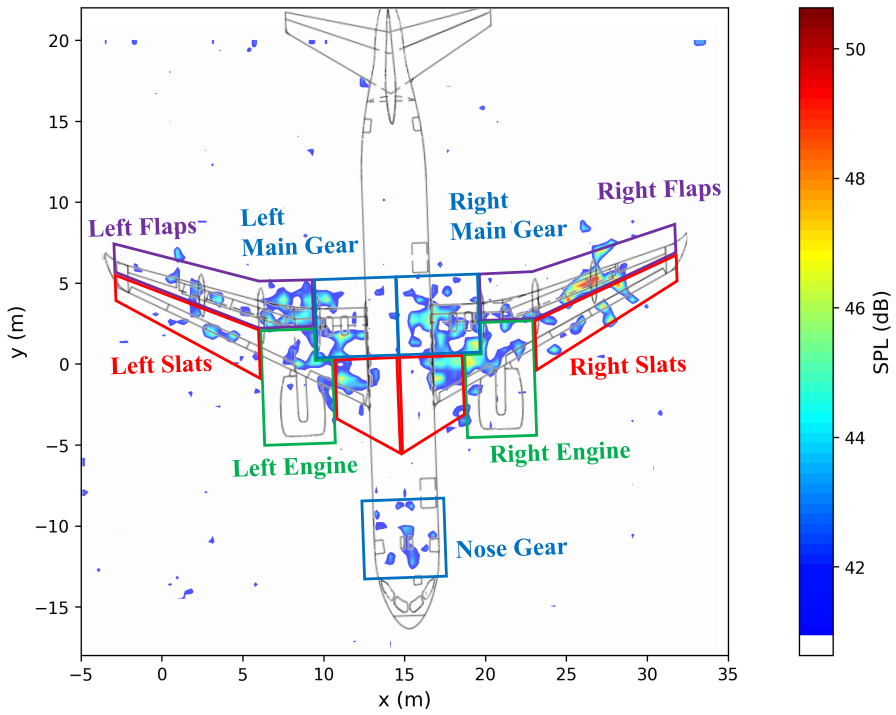

Figure 10: Definition of integration regions.

less significant under this particular flight condition. This example therefore illustrates that ROI-based integration should not be interpreted simply as a numerical ordering of source regions; instead, it provides a quantitative basis for relating localized source strengths to the aircraft configuration, flight attitude, and observer geometry discussed throughout this study.

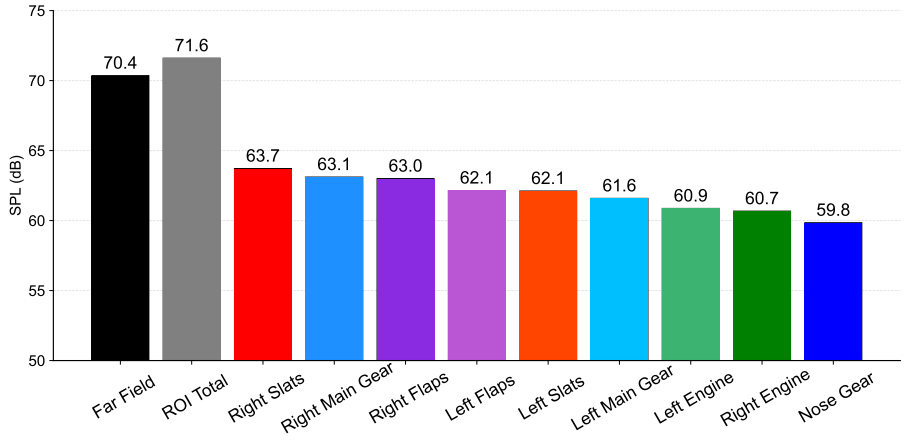

Figure 11: Regional source-level contributions at 2500 Hz.

7 CONCLUSIONS

This paper presents a practical framework for full-scale aircraft flyover measurements of large civil aircraft in China. The framework covers four main stages: microphone array design and calibration, noise acquisition, aircraft trajectory determination, and data processing. It is intended to improve the efficiency of full-scale field tests while ensuring the reliability of the key inputs required for flyover noise source localization.

Two computer vision-based techniques are introduced within the framework. First, a microphone position calibration method is used to improve field deployment efficiency while maintaining the required array positioning accuracy. Second, a two-camera trajectory determination scheme based on instance segmentation is developed to provide aircraft trajectory information for moving-source localization. Using the calibrated array geometry and reconstructed aircraft trajectory, the MCB-GT method is applied to real approach flyover noise data. For the analyzed flyover case, the resulting source maps show source distributions around the main aircraft noise-generating components, illustrating the practical applicability of the proposed framework.

Regional source-level integration is further performed on the processed source maps to quantify and compare the relative contributions of different aircraft source regions. The comparison with far-field microphone measurements provides a consistency check for the source-integration results and supports the feasibility of the proposed quantitative analysis procedure.

Overall, the proposed framework provides a practical reference for future aircraft flyover noise tests and source identification studies of large civil aircraft. Future work will focus on ground-reflection effects and atmospheric propagation compensation to further improve the quantitative accuracy and robustness of the method.

References

[1] International Civil Aviation Organization. "Reduction of noise at source." `https://www.icao.int/environmental-protection/reduction-noise-source`, 2026. Accessed on 14 April 2026.

[2] J.-F. Piet, U. Michel, and P. Böhning. "Localization of the acoustic sources of the A340 with a large phased microphone array during flight tests." In *8th AIAA/CEAS Aeroacoustics Conference*. 2002. AIAA Paper 2002-2506.

[3] U. Michel, J. Helbig, B. Barsikow, M. Hellmig, and M. Schüttpelz. "Flyover noise measurements on landing aircraft with a microphone array." In *4th AIAA/CEAS Aeroacoustics Conference*. Toulouse, France, 1998. AIAA Paper 1998-2336.

[4] U. Michel and W. Qiao. "Directivity of landing-gear noise based on flyover measurements." In *5th AIAA/CEAS Aeroacoustics Conference*. Bellevue, WA, USA, 1999. AIAA Paper 1999-1956.

[5] W. Qiao and U. Michel. "A study on landing aircraft noise based on the fly-over measurements with a planar microphone array (In Chinese)." *Acta Acustica*, 26(2), 97–103, 2001. DOI: 10.15949/j.cnki.0371-0025.2001.02.013.

[6] R. W. Stoker, Y. Guo, C. L. Streett, and N. J. Burnside. "Airframe noise source locations of a 777 aircraft in flight and comparisons with past model tests." In *9th AIAA/CEAS Aeroacoustics Conference*. 2003. AIAA Paper 2003-3232.

[7] H. Siller, M. Drescher, G. Saueressig, and R. Lange. "Fly-over source localisation on a Boeing 747-400." In *Berlin Beamforming Conference*. 2010. BeBeC-2010-13.

[8] J.-F. Blais, R. Lapointe, A. Berry, and C. Camier. "Fly-over aircraft noise measurement campaign at Montreal-Trudeau airport using a microphone array." *Proceedings of Meetings on Acoustics*, 19(1), 055084, 2013.

[9] H. Siller, T. Schumacher, and W. Hage. "Low noise ATRA – phased array measurements of jet noise in flight." In *AIAA AVIATION 2021 FORUM*. 2021. AIAA Paper 2021-2160.

[10] H. Siller, W. Hage, and T. Schumacher. "Source localisation on aircraft in flight – new measurements with the DLR research aircraft airbus 320 ATRA." In *7th Berlin Beamforming Conference*. 2018.

[11] J. W. Wong, M. G. Jones, D. M. Nark, E. H. Nesbitt, L. Brusniak, and F. T. Dockery. "Flight test methodology for NASA advanced inlet liner on 737MAX-7 test bed (Quiet Technology Demonstrator 3)." In *25th AIAA/CEAS Aeroacoustics Conference*. 2019. AIAA Paper 2019-2763.

[12] R. H. Thomas, Y. Guo, I. A. Clark, and J. C. June. "Propulsion airframe aeroacoustics and aircraft system noise flight research test: NASA overview." In *AIAA AVIATION 2022 FORUM*. 2022. AIAA Paper 2022-2993.

[13] T. Chen, H. Hou, Z. Chen, Y. Wang, and X. Li. "ARJ aircraft noise measurement from fly-over test (in Chinese)." *Acta Metrologica Sinica*, 33, 437–440, 2012. DOI: 10.3969/j.issn.1000-1158.2012.05.12.

[14] T. Chen, H. Hou, and Z. Chen. "ARJ aircraft landing gear noise characteristics from fly-over measuring (in Chinese)." *Journal of Vibration and Shock*, 31, 83–86, 2012.

[15] T. Chen, H. Hou, Z. Chen, Y. Wang, and X. Li. "Landing gear noise identification in the ARJ21 aircraft during landing stage (in Chinese)." *Acta Acustica*, 38, 615–623, 2013. DOI: 10.15949/j.cnki.0371-0025.2013.05.012.

[16] J. R. Underbrink. "Pletharrays for aeroacoustic phased array applications." *International Journal of Aeroacoustics*, 16, 202–229, 2017. DOI: 10.1177/1475472X17718884.

[17] S. Tao, C. W. Lee, and W. Ma. "Sound source localization errors caused by installation deviations of large-scale microphone arrays." *Aerospace Systems*, 2025. DOI: 10.1007/s42401-025-00363-z.

[18] Z. Zhang. "A flexible new technique for camera calibration." *IEEE Transactions on Pattern Analysis and Machine Intelligence*, 22, 1330–1334, 2000. DOI: 10.1109/34.888718.

[19] Ultralytics. "YOLO11." Available online, 2026. Accessed on 3 March 2026.

[20] H. A. Siller. "Localisation of sound sources on aircraft in flight." In *Proceedings of the Internoise 2012/ASME NCAD Meeting*. New York City, NY, USA, 2012.

[21] C. Zhang. *Key Theoretical Research on Array Imaging Method for Moving Sound Source Localization (in Chinese)*. Ph.D. thesis, Shanghai Jiao Tong University, Shanghai, China, 2025.

[22] C. Zhang and W. Ma. "Frequency-domain expression of sound pressure field radiated by monopole source with general moving trajectory." *Journal of Sound and Vibration*, 570, 118137, 2024. DOI: 10.1016/j.jsv.2023.118137.

[23] C. Zhang and W. Ma. "Deconvolution of mode composition beamforming for rotating source localization." *Aerospace Systems*, 7, 727–734, 2024. DOI: 10.1007/s42401-024-00297-y.